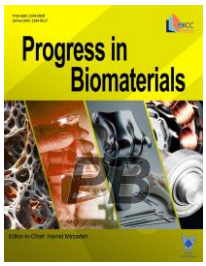

Volume 14, Issue 3, 2025: Article 13

Progress in Biomaterials (PIBM)

https://doi.org/10.57647/pibm.2025.17542

Development of Polylactic Acid/Hydroxyapatite Composite Filaments for 3D Printing of Bone Tissue Engineering Scaffolds

Bilal Cinici[1], Sule Gozonunde[2], Mustafa Kurt[3], Liviu Duta[4*], Oguzhan Gunduz[1,3*]

[1]*Center for Nanotechnology & Biomaterials Application and Research (NBUAM), Marmara University, Istanbul, 34890, Turkey.*
[2]*Department of Nanoscience and Nanoengineering, Nanotechnology Institute, Gebze Technical University, Turkey*
[3]*Department of Mechanical Engineering, Faculty of Technology, Marmara University, Turkey*
[4]*National Institute for Laser, Plasma and Radiation Physics, 409 Atomistilor Street, 077125 Magurele, Romania*

***Corresponding authors:** liviu.duta@inflpr.ro; ucemogu@ucl.ac.uk

Original Research

Received:
20 June 2025

Revised:
19 August 2025

Accepted:
30 September 2025

Published in Issue:
30 September 2025

Abstract

This study addresses the development of novel composite filaments tailored for 3D printing applications in bone tissue engineering. The granules were fabricated by blending polylactic acid (PLA) with commercial hydroxyapatite (HA) at different weight ratios of 10, 20, 30, and 40% (i.e., PLA/HA_10, PLA/HA_20, PLA/HA_30, and PLA/HA_40), using twin-screw extrusion. The resulting granules were subsequently processed into filaments through single-screw extrusion. The as-obtained filaments were comprehensively characterized in terms of thermal stability, morphological features, mechanical properties, and biological performance. It should be emphasized that the variation in HA concentration played a critical role in optimizing both the mechanical and biological performance of the composite filaments. Mechanical testing demonstrated increased elastic modulus for PLA/HA_10 and PLA/HA_20 composites. However, higher HA concentrations adversely affected the tensile strength, likely due to particle agglomeration and poor interfacial adherence between the polymer matrix and ceramic phase. In vitro biological evaluation revealed that low-to-moderate HA concentrations (i.e., 10 and 20%) improved cytocompatibility and promoted cell attachment. These findings underscore the importance of carefully tailoring the HA content to develop functional composite materials suitable for bone scaffold fabrication, with promising implications for future clinical applications in bone tissue engineering.

Keywords: 3D printing; filament; bone tissue; hydroxyapatite–biopolymer blending; biomedical applications; industry

Cite this article: Cinici, B., Gozonunde, S., Kurt, M., Duta, L., Gunduz, O., (2025). Development of Polylactic Acid/Hydroxyapatite Composite Filaments for 3D Printing of Bone Tissue Engineering Scaffolds, *Progress in Biomaterials,* 14(03), Article 13.
https://doi.org/10.57647/pibm.2025.17542

Graphical abstract

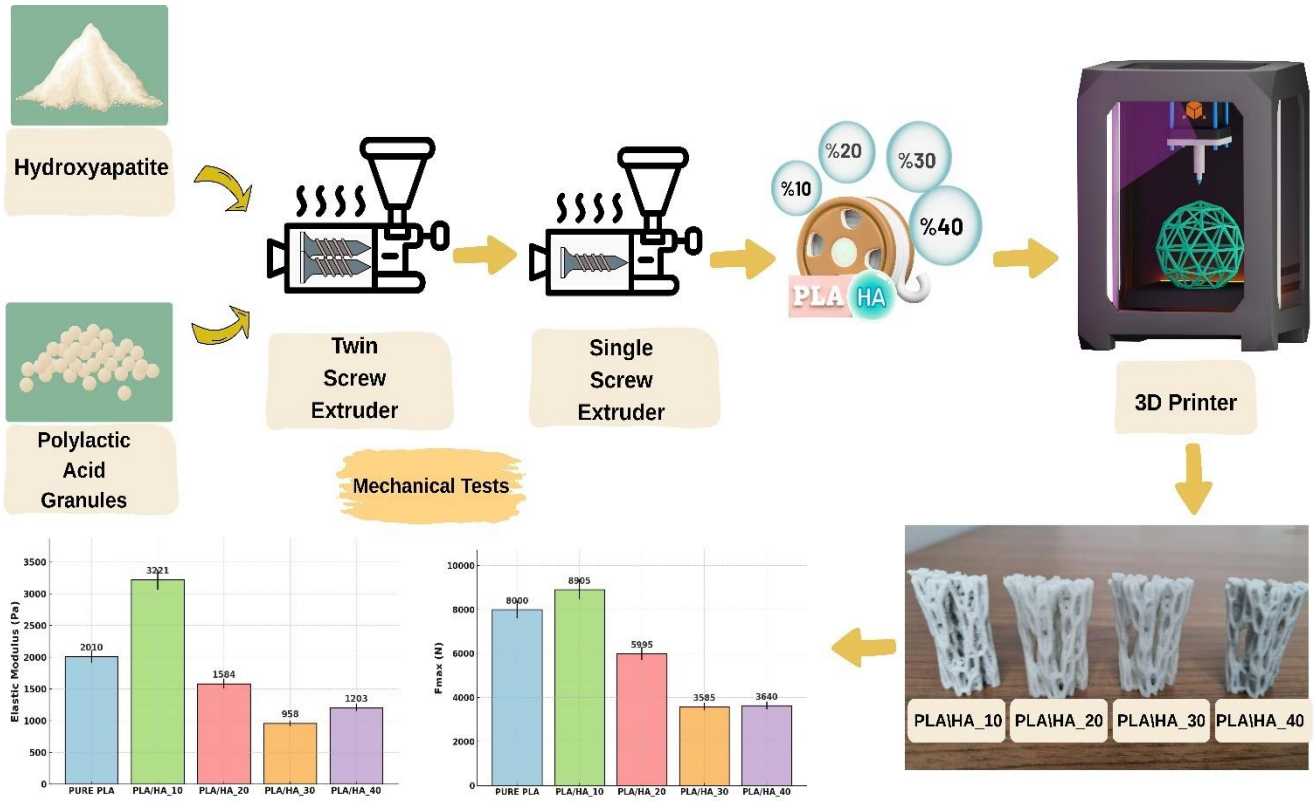

1. Introduction

Biomedical engineering, situated at the intersection of healthcare and emerging technologies, is a multidisciplinary field dedicated to improving human health and quality of life [1]. One of the most transformative advancements in this field is the integration of 3D printing technologies into biomedical applications. Among the most impactful uses is the fabrication of artificial bone tissue scaffolds, a process that underscores the critical role of additive manufacturing in modern biomedical engineering [2, 3]. However, the manufacturing of such scaffolds presents significant challenges, primarily due to the stringent requirements for biocompatibility, mechanical integrity, and patient-specific customization. In this context, 3D printing offers an unique solution, enabling the precise design and fabrication of complex, tailor-made scaffolds with controlled porosity, architecture, and material composition. Thus, the application of 3D printing technologies is pivotal in overcoming traditional limitations and advancing the development of functional bone tissue engineering constructs [4, 5, 6, 7].

It should be emphasized that bone scaffolds serve as temporary matrices that support cell growth, facilitate tissue regeneration, and ultimately promote bone repair. The effectiveness of these scaffolds is determined by several critical factors, including mechanical properties [8, 9, 10] such as strength and elasticity and biocompatibility [11, 12, 13].

Generative design plays a pivotal role in scaffold development [14, 15, 16], enabling the creation of highly porous architectures that closely resemble natural bone structures. This enhanced porosity improves scaffold durability, promotes better cell adhesion and proliferation, and optimizes mechanical performance, determining the scaffolds' suitability for load-bearing appliocations [17, 18].

These advantages significantly enhance the success and clinical applicability of artificial bone scaffolds [19]. Moreover, 3D printing technology offers precise control over scaffold fabrication, allowing the production of complex and customizable geometries that are challenging to achieve with conventional manufacturing methods [20]. This capability is particularly beneficial for regulating micro- and macro-porosity levels, which are essential for facilitating cell attachment and tissue regeneration.

Polyactic acid (PLA) is a biodegradable thermoplastic polymer that can be derived from renewable and edible

10.57647/pibm.2025.17542

resources such as corn starch and sugar cane [21]. One of the key advantages of PLA, particularly in biomedical applications, is its biocompatibility, biodegradability, and ease of processing [22, 23], which make it a suitable material for use in 3D printing technology.

Hydroxyapatite (HA), a calcium phosphate-based mineral that constitutes approximately 50-70% of the inorganic component of natural bone, is widely recognized for its suitability in artificial bone tissue scaffolds [23]. Due to its chemical similarity to the mineral phase of bone, HA promotes osteointegration – the process by which bone tissue forms a direct interface with an implant surface [23, 24].

Incorporating HA into PLA-based filaments is intended to enhance the mechanical strength of the resulting composite scaffold and to improve bioactivity, thereby facilitating more effective bone regeneration.

This research focuses on the fabrication of a novel filament intended for integration with generative design and 3D printing technologies in the production of artificial bone tissue scaffolds [25]. A detailed characterization of the PLA/HA composite filament has been conducted to assess its suitability for biomedical applications, particularly in bone tissue engineering.

The analysis includes the evaluation of critical mechanical properties, such as tensile strength, flexibility, and degradation rate, which are essential for ensuring the functional performance of bone scaffolds. In addition, the thermal and rheological properties of the composite material have been investigated to determine its compatibility with 3D printing processes.

The formulation of PLA and HA blend has been carefully optimized to achieve a favorable balance between mechanical integrity, biodegradability, and printability [26].

The production process of the composite filament, described in detail by [27], involves granulating the PLA and HA powder using a twin-screw extruder, followed by filament extrusion through a single-screw extruder. This two-step extrusion approach has been refined to ensure homogeneous dispersion of HA particles within the PLA matrix and to mentain consistent filament quality. This is an essential prerequisite for error-free 3D printing and for preserving the structural integrity of the printed scaffold [28].

Furthermore, the influence of varying HA concentrations on both the mechanical and biological properties of the resulting scaffold has been systematically investigated. However, it was demonstrated that excessive HA loading may adversely affect the printability and flexibility of the composite [29], highlighting the need to establish an optimal HA-to-PLA ratio.

Following the characterization and fabrication of the PLA/HA composite filament, the research advances to its application in 3D printing of bone scaffolds. The scaffolds were specifically designed to replicate the trabecular arhitecture of natural bone, thereby promoting cell infiltration, vascularization, and nutrient diffusion, which are key parameters for effective bone regeneration.

Recent literature [30] underscores that while numerous studies have explored polymeric scaffolds for tissue engineering, advancements in 3D and emerging 4D printing technologies have significantly expanded the design and functional capabilities of such scaffolds.

The extracellular matrix (ECM) plays a central role in guiding tissue regeneration, and 3D printing enables the fabrication of patient-specific scaffolds with complex geometries closely mimicking native ECM structures. Its seamless integration with medical imaging allows precise reproduction of anatomical shapes, while the introduction of smart materials in 4D printing adds dynamic responsiveness, enhancing the scaffold's ability to replicate the functional adaptability of natural tissues. Reviews in the field highlight the broad spectrum of biopolymers used, the growing importance of hydrogels for dynamic 4D constructs, and the critical influence of printing parameters on the mechanical, morphological, and biological performance of scaffolds.

Beyond additive manufacturing, comparative studies emphasize that no single fabrication technique universally meets all structural, mechanical, and cost-effectiveness requirements for tissue-engineered scaffolds [31].

Traditional methods such as melt molding, especially when combined with particulate leaching, offer reproducible, scalable, and low-cost alternatives. Foam injection molding, in particular, has emerged as a promising approach due to its simplicity and potential for structural control, with recent work exploring its hybridization with particulate leaching to achieve tailored porosity and architecture.

Incorporating these recent findings into the manuscript would situate the present study within the broader technological landscape, acknowledging both state-of-the-art additive manufacturing and alternative cost-effective scaffold fabrication techniques, while critically positioning the novelty of our generative design–driven, PLA/HA-based approach.

One should emphasize that, the present research aims to advance bone tissue engineering through a novel, integrative, and application-oriented approach that merges advanced material formulation with design-driven additive manufacturing.

Specifically, it introduces three original contributions: (i) the implementation of a

generative design methodology for scaffold modelling, enabling optimization of mechanical performance and porosity distribution to replicate natural bone architecture, a strategy not previously applied to PLA/HA scaffolds; (ii) the development of customized PLA/HA composite filaments with optimized extrusion parameters, ensuring reliable fabrication of structurally consistent scaffolds via fused deposition modeling and full compatibility between digital designs and physical outputs; and (iii) a holistic, multiscale characterization encompassing structural, morphological, mechanical, and in vitro biological assessments, collectively confirming the feasability of the proposed workflow for biomedical applications.

2. Materials and methods

2.1. Preparation of PLA/HA blends for the fabrication of composite filaments

To obtain PLA/HA blends with different ratios (further denoted as PLA/HA_10, PLA/HA_20, PLA/HA_30, and PLA/HA_40, according to the added HA weight), HA powder with a purity of 99.95% and a particle size of 50 nm was supplied by Nanokar (Istanbul, Turkiye). It is important to mention that the HA concentrations selected (10%, 20%, 30%, and 40 wt. %) reflect an empirically supported mid-range window widely recognized in the literature. For example, [32] reported a significant enhancement in tensile strength and elastic modulus at 15 wt.% HA loading, confirming the mechanical benefit within this range. Moreover, studies such as [33] revealed that PLA/HA scaffolds containing ≥ 20 wt % of HA achieve mechanical properties compatible with trabecular bone and effectively induce osteogenic differentiation without inflammatory effects. Accordingly, a comprehensive evaluation across the 10 to 40 wt.% range was conducted to systematically investigate the balance between mechanical integrity and in vitro biological performance.

BioPLA granules with a particle size of 3-4 mm were supplied by Resinex (Bursa, Turkiye). In the initial stage, 25, 50, 100, 150, and 200 grams of HA powder were individually added to 500 grams of PLA granules to obtain the desired PLA/HA composite formulations. Figure 1 provides a schematic representation of the complete filament fabrication process.

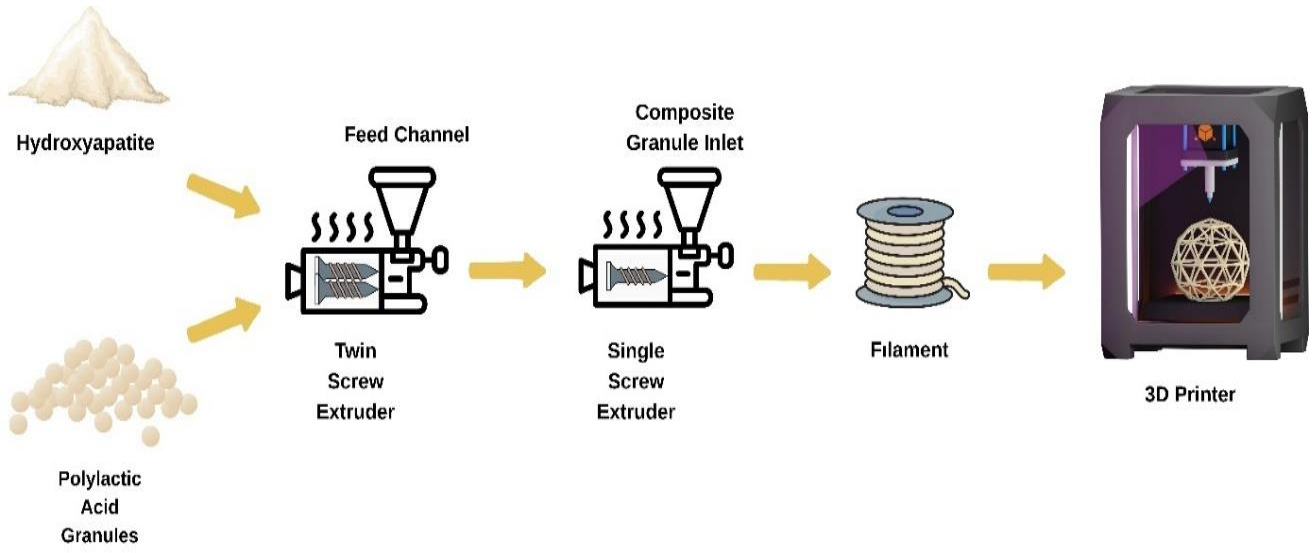

Figure 1. Schematic representation of the composite filament production process. Hydroxyapatite powder and polylactic acid granules are blended using a twin-screw extruder, followed by granule reprocessing via single-screw extrusion to produce a uniform filament. This filament is subsequently used for 3D printing of bone tissue scaffolds

The obtained PLA/HA blends were processed into PLA/HA granules using a twin-screw extrusion system (Rootex RTX-T25 twin-vial extruder brand). These granules were subsequently subjected to advanced characterization techniques, including Scanning Electron Microscopy (SEM), Fourier Transform Infrared (FTIR) Spectroscopy, Thermogravimetric Analysis (TGA), (DSC), and Differential Scanning Calorimetry (DSC), to investigate their morphological, chemical, and thermal properties. Following characterisation, the PLA granules were processed into filaments using a single-screw extruder (RTX-S16, Kökbir), designed for the production of 1.75 mm and 3 mm diameter filaments for 3D printing. The extruder features a 16 mm screw diameter and a 24 L/D ratio, parameters optimised for polymer filament production. Prior to extrusion, the PLA granules were dried at 80 °C for 4–6 h to remove residual moisture and prevent thermal degradation during compounding.

The extrusion temperature profile was set between 180 °C at the feed zone and 200 °C near the die, consistent with

10.57647/pibm.2025.17542

standard PLA processing conditions. Screw rotation speeds of 30–50 rpm were employed to ensure efficient mixing, maintain melt homogeneity, and control flow, while preventing thermal degradation.

The feed rate ranged from 1 to 2 kg/h, corresponding to an estimated residence time of 2–4 min within the extruder. The die diameter was set to 1.75 mm to match the target filament diameter for FDM 3D printing. An air knife cooling system was employed immediately after extrusion to stabilize filament dimensions and surface finish prior to winding.

All aforementioned parameters were determined through preliminary optimization trials to ensure filament dimensional stability and material integrity during extrusion. Under these conditions, five composite filament types with varying HA contents were successfully produced.

It is important to note that the decision to use a single-screw extruder for filament fabrication was based on the specific objective of this processing stage, which was not further compounding but rather the shaping of previously homogenized composite material into printable filaments. As detailed earlier in the manuscript, the blending of PLA granules with HA powder was initially performed using a twin-screw extruder to ensure uniform dispersion and effective mixing.

The resulting composite pellets were then processed using a single-screw extruder solely for filament formation, where material homogenization had already been achieved.

This approach is commonly employed when the formulation is already well-dispersed, as the single-screw system allows for more straightforward temperature control and filament diameter consistency during extrusion.

2.2. Characterization of fabricated filaments

The chemical and structural characterization of the filaments was carried out by FTIR, X-ray Diffraction (XRD), SEM, DSC, and TGA tests. The fabricated filaments were subsequently used in the production of Groid-type bone scaffolds through generative design technology.

The scaffold architectures were optimized to meet the mechanical strength and functional requirements for artificial bone tissue applications.

It is important to note that generative design constitutes a key step in scaffold development, as it enables the creation of structures with improved mechanical performance and enhanced biological functionality [25].

Five composite filament samples containing varying amounts of HA were subjected to tensile and compression tests to evaluate their mechanical properties. The specimens were prepared using custom-designed molds fabricated via 3D printing, in accordance with the ISO 527 Type A standard for tensile testing.

Additionally, this study investigated the effect of PLA composites reinforced with varying concentrations of HA on cell viability using the (3-(4,5-dimethylthiazol-2-yl)-5-(3-carboxymethoxyphenyl)-2-(4-sulfophenyl)-2H tetrazolium) (MTS) assay. The MTS test is a colorimetric method that assesses mitochondrial metabolic activity as an indicator of viable, metabolically active cells.

In the presence of living cells, MTS is bioreduced into a soluble formazan product, which can be quantified by measuring absorbance. Measurements were performed at four time points:

days 1, 7, 14, and 21. Cell viability was evaluated by measuring absorbance values, enabling a quantitative estimation of viable cell numbers at each time point.

Human osteoblast cells (hFOB 1.19) were used to evaluate the cytocompatibility of the composites. Cells cultured in standard medium without exposure to test materials served as the control group.

This setup enabled a direct comparison of cell proliferation in the presence of the composites with the baseline growth profile of untreated cells.

3. Results and discussion

3.1. Scanning Electron Microscopy (SEM)

The chemical composition and surface morphology of the PLA/HA composites were examined using SEM. Figure 2 presents the SEM micrographs of both the composite filaments and granules.

Significant morphological changes were observed with increasing HA content.

As reported by [34], pure PLA exhibits a homogeneous and smooth surface morphology. However, the incorporation of HA disrupted this homogeneity [34], indicating successful integration of the ceramic phase into the PLA matrix.

Moreover, as the HA content increased, more pronounced surface irregularities and structural distortions were observed. These morphological changes suggest enhanced interfacial interactions between the polymer and the ceramic phase, which may contribute to the improvement of the mechanical properties of the resulting composite material [35].

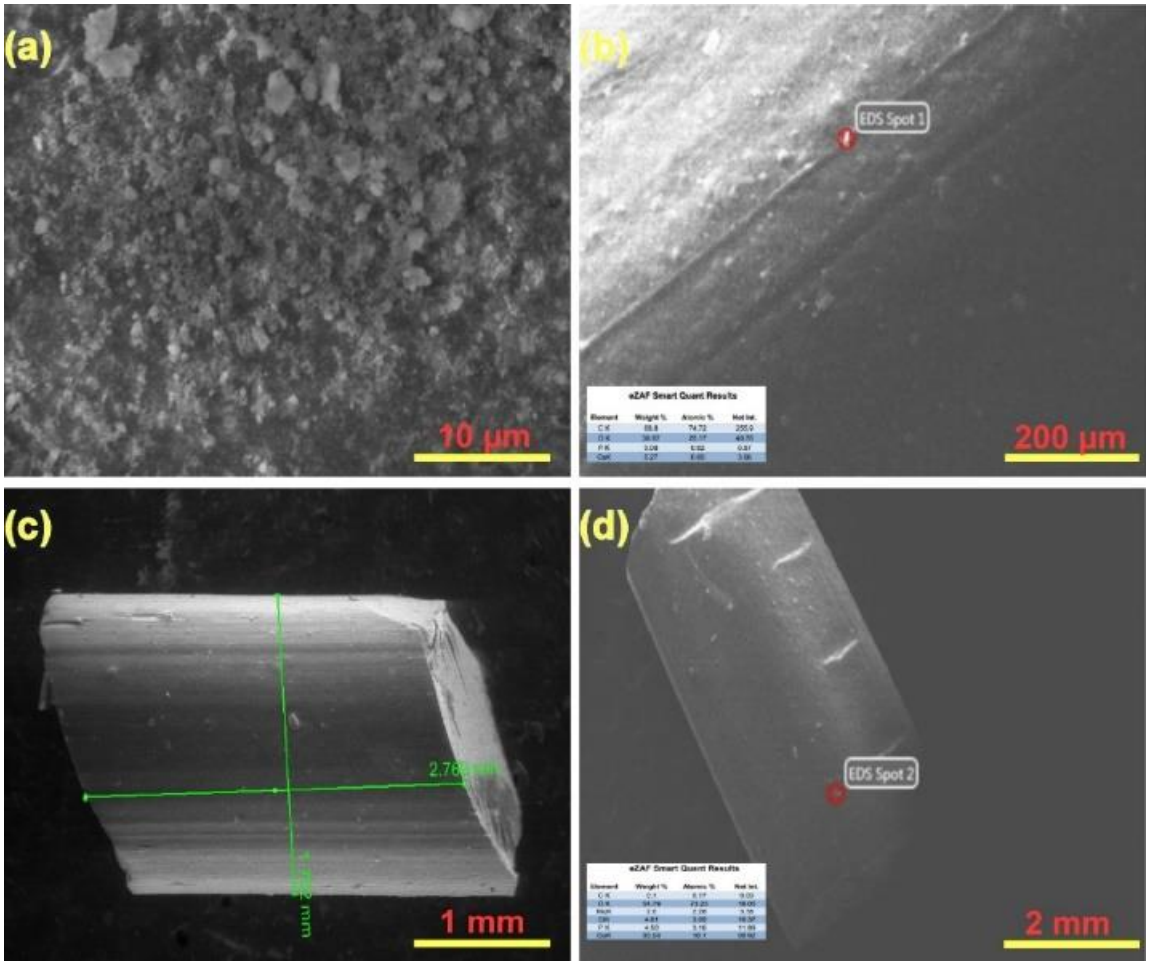

Figure 2. (a) SEM surface micrograph of the HA-doped granule sample, (b) EDS results of the HA-doped granule sample, (c) SEM surface micrograph of the HA-doped filament sample, (d) EDS results of the HA-doped filament sample

3.2. Energy Dispersive X-Ray Spectroscopy (EDS)

EDS analysis revealed that the PLA matrix predominatly contained carbon and oxygen, confirming its organic composition. In contrast, the HA phase was characterized by the presence of calcium and phosphorus, consitent with the typical elemental constituents of HA. Moreover, trace amounts of magnesium and silicon were detected, which are presumed to originate from impurities and inorganic secondary compounds associated with the HA additive. SEM-EDS results indicated that homogeneous granular structures were successfully achieved through the use of a twin-screw extruder. Such uniformly dispersed composites are considered highly suitable for biomedical applications, due to their improved structural integrity and compositional consistency.

3.3. Fourier Transform Infrared (FTIR) Spectroscopy

FTIR analysis of PLA granules doped with HA at various doping levels (PLA/HA_10, PLA/HA_20, PLA/HA_30, and PLA/HA_40) is shown in Figure 3. The FTIR spectra reveal structural changes and interfacial interactions between PLA and HA. In the case of PLA/HA_10 composite, characteristic absorption bands were observed at 2945 cm^{-1} (C–H stretching), 1749 cm^{-1} (ester carbonyl groups) and 1180 cm^{-1}, 1126 cm^{-1} and 1080 cm^{-1} (C–O–C streching vibrations). The appeareance of additional peaks at 602 cm^{-1} and 565 cm^{-1} confirms the incorporation of HA, coresponding to phosphate group vibrations. Furthermore, new bands at 1267 cm^{-1} and 866 cm^{-1} suggest possible molecular interactions between the PLA matrix and HA particles. In the case of PLA/HA_20 composite, the FTIR spectra show no additional peaks; however, slight changes in peak intensities and minor shifts in wavenumbers are observed. These variations, particularly in the regions around 2994 cm^{-1} (C–H stretching), 1682 cm^{-1} (ester carbonyl groups), and 600–560 cm^{-1} (phosphate-related groups), may be attributed to intermolecular interactions between the PLA matrix and the HA filler. In the case of PLA/HA_30 composite, the phosphate-related bands become more pronounced at 602 cm^{-1}, 563 cm^{-1}, 476 cm^{-1}, and 415 cm^{-1}, while the characteristic peaks of PLA (e.g., 2995 cm^{-1} for C–H and 1749 cm^{-1} for ester groups) remain clearly detectable. This indicates that the incorporation of HA at higher loadings enhances the

10.57647/pibm.2025.17542

spectral contribution of phosphate groups while maintaining the structural integrity and compatibility of PLA within the composite system. In the case of PLA/HA_40 composite, HA becomes the dominant phase, as evidenced by intensified phosphate bands at 563 cm^{-1}, 474 cm^{-1}, and 414 cm^{-1}, along with OH^--related peaks at 866 cm^{-1} and 754 cm^{-1}. Nevertheless, the main functional groups of PLA, such as C–H (2995 cm^{-1}) and C–O–C streching vibrations (1182 cm^{-1}, 1081 cm^{-1}, 1026 cm^{-1}), are still preserved. Comparative analysis across different doping levels indicates that increasing the HA content enhances both the dispersion and the spectral prominence of HA-related bands, reflecting stronger interfacial interactions. Importantly, the chemical integrity of the PLA matrix is preserved, demonstrating the formation of a homogeneous and stable composite structure. These results suggest that higher HA doping levels improve the functional properties of the material, thereby increasing its potential for advanced biomedical applications.

3.4. Thermogravimetric Analysis (TGA)

The thermal degradation behavior of pure PLA granules and PLA/HA composites, in both granule and filament forms, was systematically evaluated using TGA/DTG analysis.

The key thermal degradation parameters temperature at 5% weight loss ($T_{5\%}$), max. degradation rate, temperature at max. rate of degradation (T_{max}), total mass loss, and residual product at 500°C are summarized in Table 1, while the corresponding graphical representations are provided in Supplementary Figures S1, S2, and S3. The TGA of the pure PLA granules and the PLA/HA composite granules and filaments revealed distinct trends related to the incorporation of HA and the material's processing form.

The pure PLA granules exhibited the lowest thermal residue and a high onset degradation temperature, consistent with the absence of inorganic reinforcements and the homogeneous nature of the polymer [36].

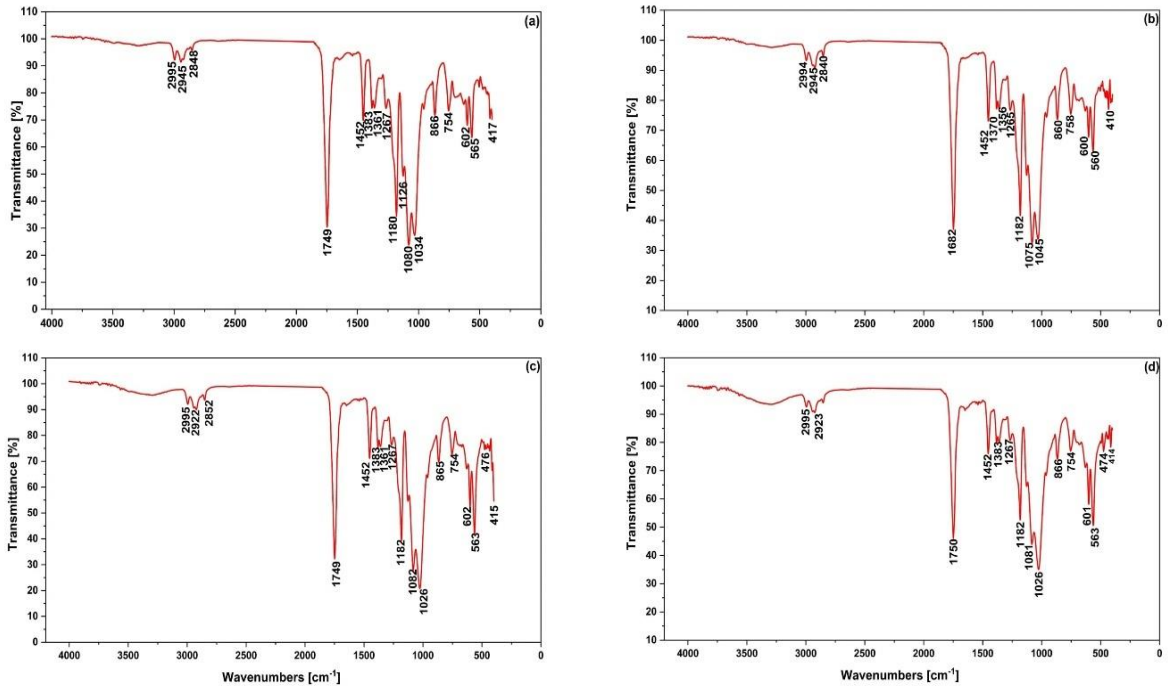

Figure 3. FTIR spectra of PLA granule samples with varying HA content: (a) PLA/HA_10, (b) PLA/HA_20, (c) PLA/HA_30, and (d) PLA/HA_40

Table 1. Summary of the thermal degradation parameters obtained from TGA/DTG analysis of pure PLA granules and PLA/HA composites, in both granule and filament forms

Material form	Sample code	$T_{5\%}$ [°C]	Max. degradation rate [mg/min]	T_{max} [°C]	Total mass loss [%]	Residual product [%]
Granules	Pure PLA	297.8	6.284	379.2	99.1	0.9
	PLA/HA_10	311.5	5.580	381.0	90.9	9.1
	PLA/HA_20	283.2	7.603	391.5	82.7	17.3
	PLA/HA_30	197.2	4.526	391.4	73.3	26.7
	PLA/HA_40	314.4	5.032	393.6	67.6	32.4
Filaments	PLA/HA_10	325.2	6.712	386.5	90.9	9.1
	PLA/HA_20	300.6	4.978	389.6	81.1	18.9
	PLA/HA_30	302.9	3.902	388.6	74.1	25.9
	PLA/HA_40	286	2.760	395.8	66.8	33.2

10.57647/pibm.2025.17542

Among the PLA/HA granules, PLA\HA_10 and PLA\HA_40 samples showed higher thermal resistance at the onset of degradation, while samples PLA\HA_20 and especially PLA\HA_30 degraded earlier, indicating possible differences in HA dispersion or interactions with the polymer matrix. Sample PLA\HA_20, despite its earlier degradation onset, displayed the highest degradation rate, which may be associated with localized thermal acceleration due to catalytic HA domains. The increasing residual content across PLA\HA_10 – PLA\HA_40 samples correlates with increasing HA content, confirming the influence of the inorganic phase on char formation. It should be noted that, even though the thermal degradation data for pure PLA filaments is not presented, based on the TGA analyses of similar materials, the basic decomposition temperatures of PLA in granule and filament forms are generally comparable. As reported in the literature [37], the filament form may exhibit a slightly lower decomposition onset ($T_{5\%}$) typically a few degrees Celsius due to chain scission and increased moisture absorption occurring during melt processing. These effects result from the thermal and mechanical stresses imposed during extrusion, which may slightly reduce the molecular weight and thermal stability of the polymer. In the case of the filaments, the onset of degradation shifted to higher temperatures for most formulations compared to their granule counterparts, suggesting enhanced thermal stabilization potentially due to improved HA distribution or structural reorganization during melt processing. Notably, PLA\HA_10 sample showed the highest thermal stability among the filaments, while sample PLA\HA_40 exhibited the lowest degradation onset but retained the highest residual mass, mirroring trends observed in the granules. As expected, a reduction in the total mass loss with increasing HA content was observed for all PLA\HA composites, both in granule and filament forms (Table 1). The consistent increase in residue content across both forms, from PLA\HA_10 to PLA\HA_40 samples, reflects the progressive integration of HA, which, while improving thermal resistance at high temperatures, tends to reduce the onset thermal stability of the composites. These results highlight the trade-off between early-stage thermal resistance and residual stability, influenced both by composition and processing history.

3.5. Differential Scanning Calorimetry (DSC) analyses

The DSC results for PLA/HA composites, in both granule and filament forms, with varying HA contents (10–40 wt.%) are summarized in Table 2 and illustrated in Figures S4 and S5. In the case of granules, across all compositions, the glass transition temperature (T_g) remains within the range of 58.6–60.5 °C, while the crystallization temperature (T_c) shows only a slight variation between 92.2 °C and 95.0 °C. These findings indicate that HA incorporation has minimal influence on the amorphous-to-crystalline transition of the PLA matrix. The most pronounced change is observed in the melting behavior of PLA/HA_40 composite, which exhibits an additional low-temperature melting peak at 109.5 °C. This feature suggests increased structural heterogeneity within the matrix and the possible coexistence of multiple crystalline phases.

Table 2. Thermal transition parameters (glass transition temperature –T_g, crystalization temperature – T_c, melting peaks – Tm_1, Tm_2) of PLA/HA composite granules and filaments with varying HA contents, as determined by DSC analysis

Material form	Sample code	T_g [°C]/[mW]	T_c [°C]/[mW]	Tm_1 [°C]/[mW]	Tm_2 [°C]/[mW]	Notable features
Granules	*PLA/HA_10*	60.5 / –2.764	92.2 / –1.683	146.4 / –3.809	154.6 / –4.952	Dual melting peaks
	PLA/HA_20	58.6 / –2.898	94.7 / –0.684	141.9 / –3.904	152.1 / –5.554	Slightly reduced Tm
	PLA/HA_30	58.8 / –2.020	95.0 / –1.019	141.1 / –2.902	149.5 / –3.968	Additional high–Tm peak
	PLA/HA_40	59.3 / –2.970	92.2 / –1.683	109.5 / –2.786	148.9 / –5.363	Low-Tm peak → heterogeneity
Filaments	*PLA/HA_10*	60.5 / –1.690	100.4 / –0.709	146.2 / –2.603	154.6 / –3.569	Dual melting peaks
	PLA/HA_20	59.3 / –3.844	92.8 / –2.699	130.7 / –3.935	151.9 / –5.722	Slightly reduced Tm_2
	PLA/HA_30	59.3 / –2.970	92.2 / –1.683	109.5 / –2.786	148.9 / –5.363	Low-Tm peak present
	PLA/HA_40	59.6 / –3.597	89.8 / –2.549	110.4 / –3.457	148.9 / –5.540	Low-Tm peak, broader melting region

10.57647/pibm.2025.17542

These trends are consistent with findings reported in the literature. For instance, [38] investigated PLA/HA composites with HA contents between 1 wt.% and 4 wt.% and observed minimal changes in T_g and T_c, in agreement with our present study. In both cases, moderate HA loadings did not substantially influence the glass transition or crystallization behavior. However, at higher HA concentrations, [38] reported the emergence of additional melting peaks, which they attributed to filler-induced matrix heterogeneity and the formation of multiple crystalline phases. This observation aligns with our results for PLA/HA_40 composite, where the low-temperature melting peak likely originates from modifications in crystalline morphology and enhanced polymer–filler interactions. Overall, the results indicate that while T_g and T_c remain relatively unaffected by HA incorporation, higher filler contents can alter the melting profile, with potential implications for processing behavior and final material performance. The DSC analysis of PLA/HA composite filaments reveals thermal behavior trends comparable to those observed in the granule form. The T_g values of the filaments range from 59.3 to 60.5 °C, while the T_c ones vary between 89.8 and 100.4 °C. The slightly lower T_c values observed in the filaments – ~3–5 °C reduction are likely attributable to differences in thermal history introduced during the extrusion process. Most filament compositions exhibit dual melting peaks, with Tm_1 ranging from 109.5 to 146.2 °C and Tm_2 from 148.9 to 154.6 °C. For instance, in the PLA/HA_30 sample, Tm_1 is observed at 109.5 °C. In comparison, [39] reported Tm_1 values of 110–120 °C and Tm_2 values of 150–155 °C for PLA/HA composites in granule form. This comparison suggests that the filament drawing and extrusion processes tend to reduce Tm_1, while Tm_2 remains relatively unaffected.

The low-temperature melting peaks observed in PLA/HA_30 and PLA/HA_40 samples (Tm_1 ≈ 109.5–110.4 °C) suggest increased heterogeneity in the crystalline phase, potentially due to filler-induced polymorphism. Similarly, [39] reported broader melting regions and enhanced crystalline heterogeneity in PLA/HA composites, attributed to the effects of filler content and thermal processing conditions.

In summary, filament processing induces polymer chain orientation and modifications in lamellar thickness, resulting in reduced crystallization temperatures and more heterogeneous melting behavior compared to the granule form. These findings are consistent with the observations reported by [38] and [39].

3.6. X-Ray Diffraction (XRD)

Figure 4 shows the XRD patterns of HA-doped PLA granule samples. The characteristic diffraction peaks of pure HA were observed at 2θ = 25.95°, 31.51°, 39.70°, 46.78°, and 48.00°, confirming the presence of the HA phase within the composite structure. In comparison, the PLA spectrum exhibited its most prominent diffraction peaks at 2θ = 17° and 19°, which are consistent with the semicrystalline nature of the PLA matrix. Upon incorporation of HA into the PLA matrix, an increase in the overall crystallinity of PLA was observed, accompanied by an enhancement in the intensity of HA-related diffraction peaks. This behavior indicates the coexistence of both amorphous and crystalline domains within the composite.

These results suggest that HA doping not only promotes the dispersion and integration of HA within the PLA matrix but also alters the structural organization of the composite material.

XRD analysis therefore represents a valuable technique for elucidating the crystal structure, assessing the degree of crystallinity, and characterising phase distribution in such composite systems.

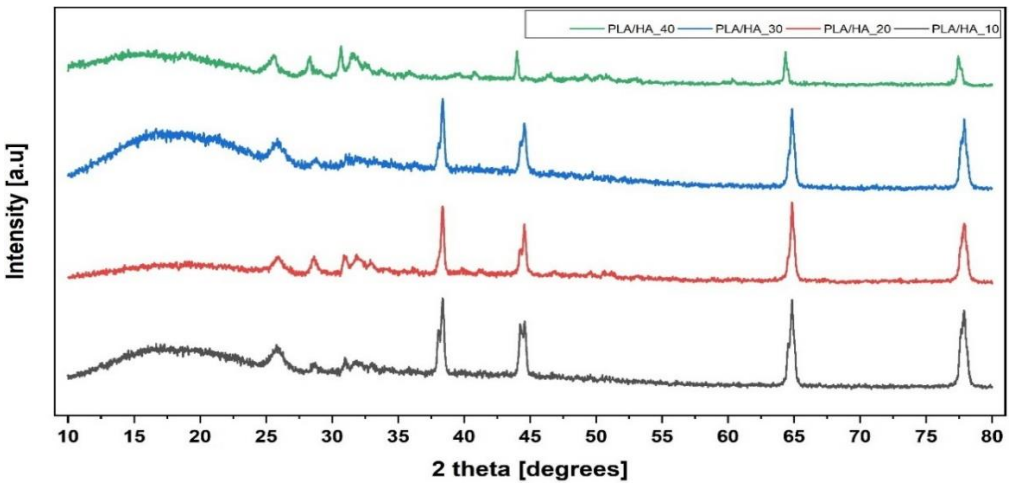

Figure 4. X-ray diffraction patterns of PLA filaments containing varying concentrations of HA: PLA/HA_10, PLA/HA_20, PLA/HA_30, and PLA/HA_40

10.57647/pibm.2025.17542

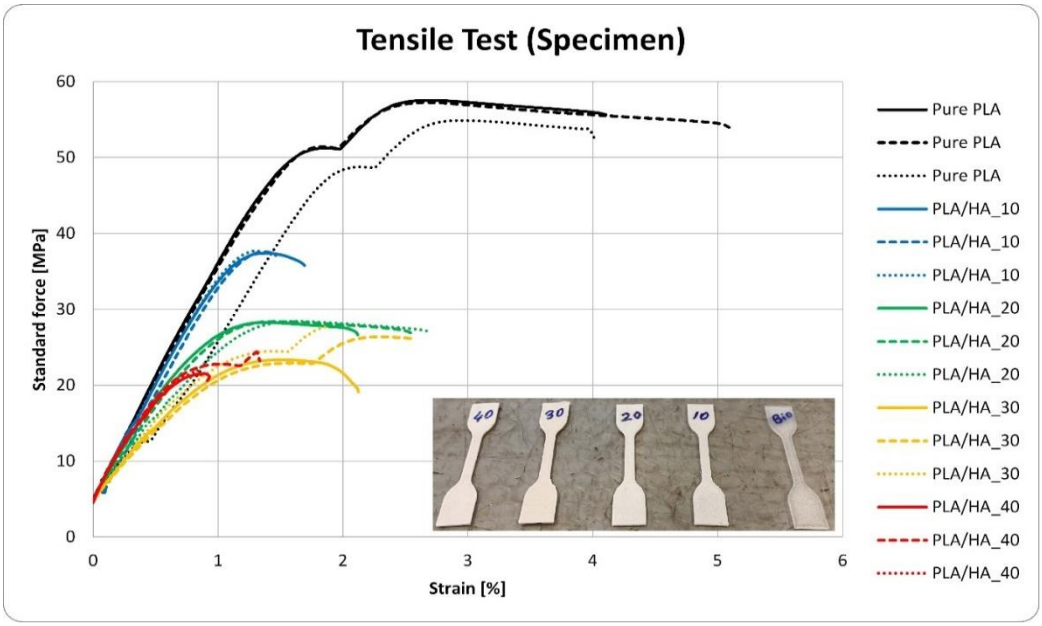

Figure 5. Tensile test results of pure (Bio) PLA and PLA specimens with varying HA contents (10%, 20%, 30%, and 40%). Inset: image of the corresponding fabricated specimens

3.7. Mechanical testing

3.7.1. *Tensile tests*

Figure 5 shows the tensile test results of pure and HA-doped PLA specimens. The analysis demonstrates that tensile strength decreases progressively with increasing HA content. Owing to the inherent elasticity of the PLA polymer matrix, the PLA/HA_10 specimens exhibit the highest tensile strength, whereas the PLA/HA_40 ones shows the lowest. These results indicate that HA incorporation significantly affects the mechanical performance of the composite, most likely due to reduced polymer chain mobility and increased structural heterogeneity at higher filler loadings. Among the different PLA/HA compositions, the PLA/HA_10 specimens exhibited the highest tensile strength. This suggests that a lower HA content is more effective in enhancing the tensile properties of the composite material, most likely due to improved filler dispersion and stronger interfacial bonding, without substantially disrupting the continuity of the polymer matrix.

The tensile strength of the PLA/HA_20 and PLA/HA_30 specimens exhibited variabilty, which may be attributed to the excessive filler–matrix interactions and partial agglomeration of HA within the polymer matrix. The PLA/HA_40 specimens showed the lowest tensile strength, indicating that higher filler content significantly disrupts matrix continuity and weakens mechanical performance. At lower additive concentrations (particularly 10% and 20%), the elastic region of the tensile stress-strain curve was more pronounced, suggesting improved energy absorption capacity and ductility. In contrast, the PLA/HA_30 and PLA/HA_40 specimens displayed shorter elastic regions and premature failure. Overall, the PLA/HA_10 specimens demonstrated the most favorable mechanical performance in both compressive and tensile tests, reflecting optimal interfacial bonding and homogeneous filler dispersion within the PLA matrix.

However, with increasing HA content (*i.e.*, PLA/HA_30 and PLA/HA_40 specimens), a marked reduction in mechanical strength was observed. This decline can be primarily attributed to the non-uniform distribution of HA particles within the PLA matrix, which promotes the formation of microvoids and stress concentration sites, thereby compromising the structural integrity of the composite.

As a result, the PLA/HA_10 specimens demonstrated superior durability and flexibility, rendering them more suitable for the fabrication of bioceramic scaffolds where mechanical resilience is essential. In contrast, higher HA loadings may be advantageous for applications that require increased brittleness or controlled mechanical degradation.

3.7.2. *Compression tests*

The compression test results of PLA specimens containing different HA contents are presented in Figure 6. Among the tested compositions, the PLA/HA_10 specimens exhibited the highest compressive strength. This suggests that at lower additive concentrations, the composite maintains a more homogeneous microstructure, which contributes to improved mechanical performance.

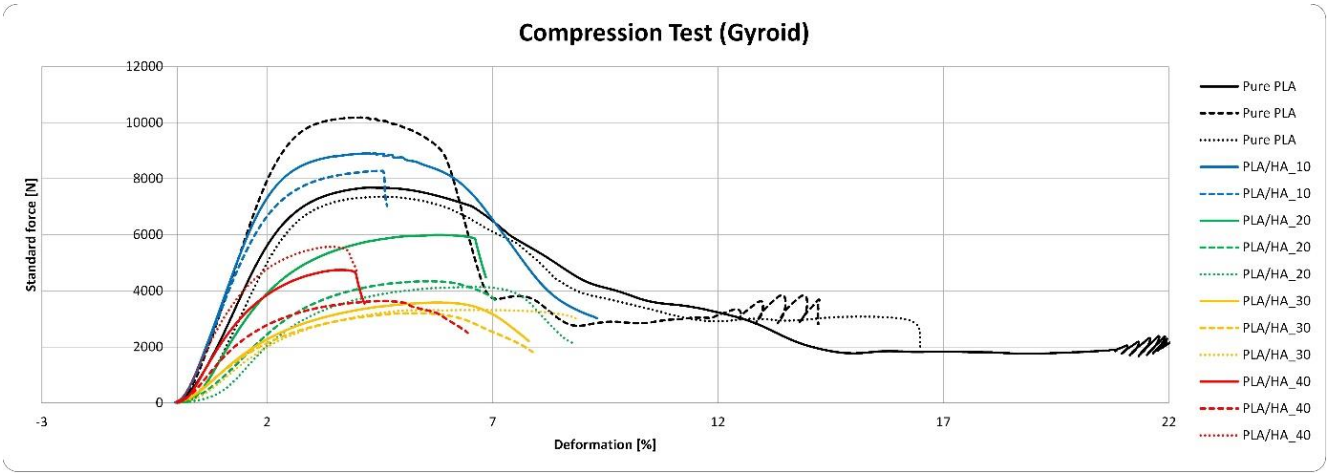

Figure 6. Compressive test results of pure (Bio) PLA and PLA specimens with varying HA content (10%, 20%, 30%, and 40%)

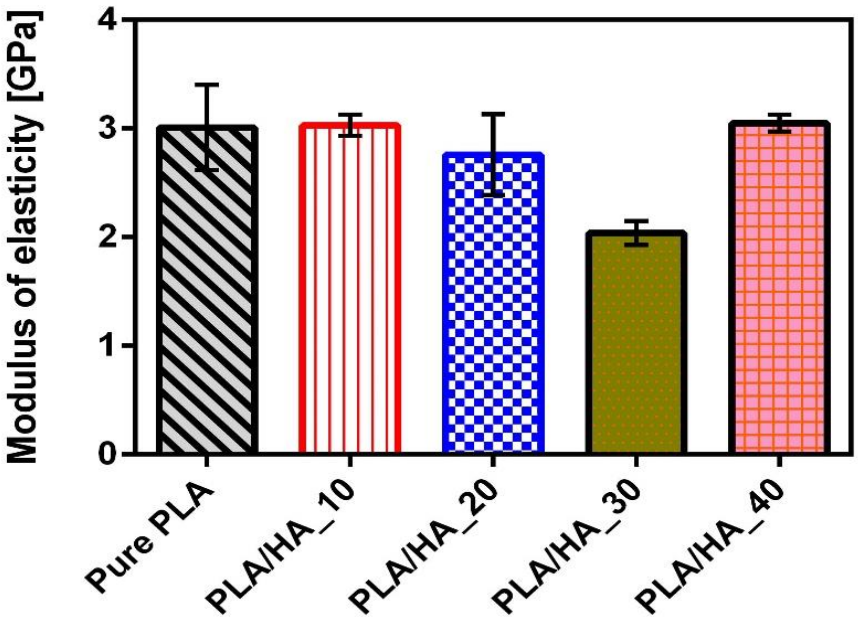

Figure 7. The tensile modulus of elasticity corresponding to pure PLA and PLA specimens with varying concentrations of HA (10%, 20%, 30%, and 40%)

At this level, the uniform distribution of HA particles likely facilitates efficient stress transfer within the matrix, thereby enhancing the overall compressive properties of the material. The compressive strength values of PLA/HA_20 and PLA/HA_30 specimens are lower than those of the PLA/HA_10 specimens.

The increase in HA content beyond a certain threshold contributes to increased brittleness and hinders the homogeneous dispersion of HA particles within the PLA matrix.

Although pure PLA is generally expected to exhibit superior durability, the PLA/HA_10 specimens demonstrated enhanced mechanical performance, likely due to a more homogeneous filler distribution and improved stress transfer efficiency. Additionally, slight variations in the mechanical performance of pure PLA may be attributed to inconsistencies during material preparation or testing. Although HA contributes minimally to micro-reinforcement, its incorporation generally increases the brittleness of the composite.

The significantly reduced compressive strength of the PLA/HA_40 specimens underscores the detrimental impact of excessive filler loading, which compromises matrix integrity and diminishes the mechanical resistance of the composite.

These findings underscore the importance of optimizing the HA content to balance mechanical strength and structural reliability in PLA-based composites.

As the HA content increases, the percentage of deformation decreases, indicating a reduction in material flexibility and an increase in brittleness.

Analysis of the tensile test results revealed that the elastic modulus remained relatively stable across most additive ratios (Figure 7). In particular, the PLA/HA_10,

10.57647/pibm.2025.17542

PLA/HA_20, and PLA/HA_40 specimens showed no significant differences in the elastic modulus, with the small variations observed likely falling within the margin of experimental error. However, the PLA\HA_30 specimens exhibited a notable decrease in elastic modulus. This behavior suggests that the additive has only a limited influence on the matrix up to a critical concentration, beyond which the elastic properties deteriorate when the additive content exceeds 30 wt.%. Possible mechanisms underlying this decline include phase separation, void formation, or a reduction in the structural integrity of the polymer matrix.

Evaluating the elastic modulus through compression testing of gyroid structures poses significant methodological challenges. These arise primarily from the non-uniform and complex geometry of the specimens. Traditional methods for determining elastic modulus rely on specimens with a constant cross-sectional area, a condition not met by gyroid architectures. The continuously varying geometry affects load distribution and deformation behavior which are influenced by both topological optimization and the intrinsic properties of the base material. As a result, conventional analytical approaches are inadequate for accurately capturing the elastic response. To overcome these limitations, Finite Element Analysis (FEA) was employed to provide a more reliable estimation of the mechanical behavior and elastic properties of the gyroid structures.

It is important to mention that the mechanical characteristics demonstrated in the current work are in accordance with other results on PLA-based scaffolds fabricated using FDM and gas foaming techniques. Thus, in a recent study [40], 3D printing technology was employed to fabricate nanocomposite scaffolds based on PLA and HA. PLA was functionalized with itaconic anhydride (PLAf) via radical grafting to enhance its affinity for the inorganic nanofiller and accelerate hydrolytic degradation. The compressive modulus of the PLA/HA 10% composite was ~ 684 MPa, while that of the PLAf/HA 10% formulation increased to about 914 MPa. This was attributed to the improved interfacial interaction between HA and the polymer matrix. The authors emphasized that the mechanical behavior of the fabricated scaffolds met the requirements for spongy (trabecular) bone but remained insufficient for applications requiring cortical bone strength [41].

[9] also reported on the fabrication of composite scaffolds composed of PLA and nano-HA (n-HA) using the fused deposition modeling (FDM) technique. PLA and n-HA were mixed in equal mass ratios to simulate the organic and inorganic phases of natural bone. Mechanical testing revealed that the PLA scaffold behaved as an elastic material, with no visible cracking under compression. In contrast, the PLA/n-HA composite exhibited brittle behavior, with scaffold rupture occuring upon compression. As a result, the compressive strength decreased from 35.41 MPa (pure PLA) to 17.80 MPa (PLA/n-HA composite). Despite the reduction in strength, the composite scaffolds displayed mechanical properties within the range of natural trabecular bone. Moreover, the incorporation of n-HA effectively mimicked the inorganic phase of bone, supporting the potential of PLA/n-HA composites for both load-bearing and non-load-bearing biomedical applications.

In the study of [42], PLA scaffolds were fabricated using a combined technique involving FDM followed by batch gas foaming. Three different types of samples were produced: (i) solid FDM samples, (ii) foamed injected samples, and (iii) foamed FDM samples. The obtained results demonstrated that the foaming process significantly affected the dimensional accuracy of both injected and FDM samples. However, the dimensional accuracy of the foamed FDM samples was considerably higher than that of the foamed injected samples. It was also important to observe that the porosity of the solid FDM samples could be controlled by changing the infill percentage. Therefore, the batch foaming procedure significantly enhanced the porosity of both injected and FDM samples up to 267%, 43%, and 21% at infill percentages of 100%, 80%, and 60%, respectively. One should note that an increased reproducibility and dimensional accuracy could be obtained in our work, in the absence of post-processing.

In this respect, a key advantage of the generative design methodology resides in preserving both mechanical integrity and geometrical fidelity without additional thermal or chemical treatments.

In another study, a combined 3D printing and gas foaming approach to fabricate bone tissue engineering scaffolds with a hierarchical, bone-like structure was also demonstrated [43].

Using response surface methodology (RSM), the authors optimized key process parameters, such as saturation pressure (55 MPa), foaming time (40 s), and temperature (68 °C), to achieve scaffolds that balanced dimensional fidelity, geometric precision, and mechanical strength. Mechanically, the optimized scaffolds demonstrated strength and structural integrity suitable for supporting cell growth, indicating that the tailored processing conditions effectively contributed to scaffold robustness. The interplay between printing precision and controlled foaming enabled the fabrication of scaffolds with mechanical properties tailored to meet the specific requirements of bone tissue applications.

10.57647/pibm.2025.17542

Rasouli and collaborators [44] combined fused filament fabrication (FFF) with a batch foaming process to engineer PLA scaffolds exhibiting a hierarchical porosity architecture. By adjusting the infill percentage via FFF, they achieved macro-pores exceeding 100 µm. The batch foaming further introduced nano-pores within the FFF scaffolds and micro-pores in injection-molded samples, resulting in a bimodal pore structure. In injection-molded foamed scaffolds, large pores > 10 µm and small pores in the range of 3–10 µm were observed, demonstrating the method's capacity to fine-tune structural heterogeneity. Consistent with the well-established influence of pore architecture on mechanical properties, the hierarchical porosity observed in the scaffolds had a significant impact on their fracture behavior. Injection-molded foamed scaffolds displayed a mixed brittle–ductile fracture mode, as revealed by Charpy impact testing. In contrast, FFF-foamed scaffolds, with their nano-scale porosity, exhibited a pure ductile fracture mechanism along pore boundaries. Notably, scaffolds produced with 60 % infill and foamed via FFF showed a remarkable impact strength increase of 72 %, from 118.2 to 202.8 J/m², highlighting the enhanced toughness achieved through this processing strategy.

One should note that the scaffold fabrication approach presented in the current work, based exclusively on filament-based 3D printing, does not rely on microporosity induced through gas foaming, yet achieves mechanical properties within a comparable range. The incorporation of HA at increasing weight fractions – up to 40 wt.% enabled the mechanical performance of the printed constructs to be finely tuned, without the need for additional post-processing treatments. Thus, in our experimental results, pure PLA exhibited a tensile strength of ~ 56 MPa. Among the composites, the PLA/HA_10 formulation demonstrated the highest tensile strength, reaching ~ 38 MPa. In compression tests, the PLA/HA_10 sample sustained a maximum load of ~ 9,400 N. Given the sample's bottom base diameter of 4 cm corresponding to a cross-sectional area of ~ 1,257 mm² the resulting compressive strength was calculated to be ~ 7.5 MPa. This value falls within the typical compressive strength range of natural trabecular bone (2–12 MPa) and is consistent with values reported in the literaure for PLA/HA composites. Although the compressive modulus and strength values fall within the ranges documented in the literature, these comparisons should be interpreted with caution due to variations in testing conditions and sample geometries.

Lastly, it is important to highlight that the integration of a generative design framework enabled precise modulation of the macrostructural features, thereby contributing to optimized mechanical integrity. This design-driven strategy could provide a controlled and reproducible alternative to gas foaming techniques, which were shown sensitive to processing parameters and environmental conditions. It is also worth emphasizing that the preservation of structural stability and geometrical precision is critical for clinical translation, particularly in load-bearing bone tissue engineering applications.

3.7.3. *In Vitro Biological Evaluation*

Figure 8a,b shows the cell viability and corresponding absorbance values of different PLA/HA composites, as determined by the MTS assay, at four time points: days 1, 7, 14, and 21.

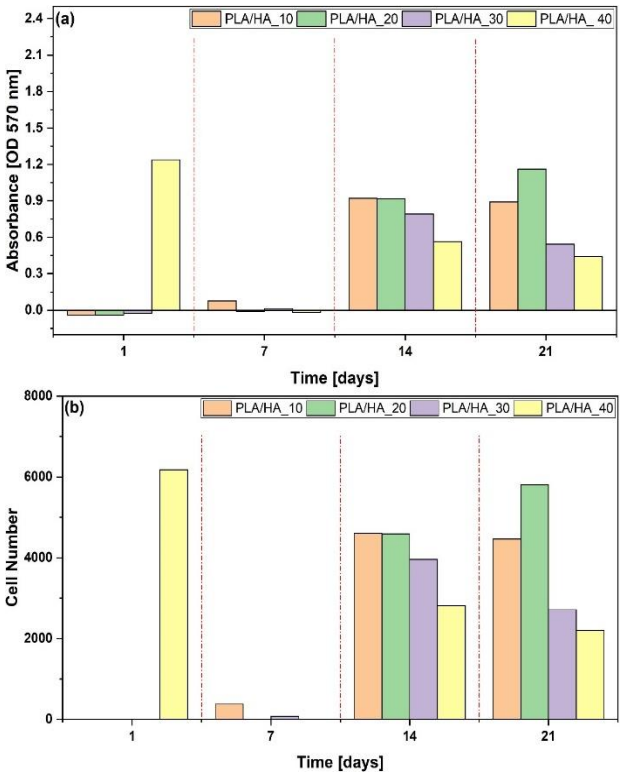

Figure 8. Absorbance values (a) and corresponding cell viability (b) of different PLA/HA composites, as determined by the MTS assay, at four distinct time points: days 1, 7, 14, and 21

Analysis of Cell Viability based on Absorbance Measurements:

On days 1 and 7, all groups exhibited either negative or near-zero absorbance values (Figure 8a). In contrast, the PLA/HA_40 samples showed a markedly higher absorbance value (Figure 8a), which is likely a transient response associated with early-stage cell adhesion on the material surface.

On day 14, both PLA/HA_10 and PLA/HA_20 samples exhibited peak absorbance values (Figure 8a), suggesting that these formulations provide a more favorable environment for cell proliferation and metabolic activity compared to the other PLA/HA composites.

This effect is likely attributable to an optimal HA content that enhances bioactivity while avoiding the negative impact of excessive mineral phase on cell–material interactions. By day 21, a marked increase in absorbance values was observed for the PLA/HA_20 samples, which exhibited the highest value among all groups (Figure 8a). The PLA/HA_10 samples also showed favorable performance, whereas the PLA/HA_30 and PLA/HA_40 samples displayed only modest increases (Figure 8a).

It should be noted that the absorbance value of the control group indicated minimal cell viability.

Assessment of Cell Proliferation via Enumeration:

The live cell count data corroborated the absorbance results, confirming the observed trends in cell viability across the tested groups (Figure 8b).

On day 1, the PLA/HA_40 composites exhibited the highest cell viability among all tested samples (Figure 8b). This finding suggests that most of the other composites lacked sufficient surface compatibility to support initial cell attachment and viability within the first 24 hours.

On day 7, cell viability remained low across all groups. However, slight increases were observed in the PLA/HA_10 and PLA/HA_30 composites (Figure 8a). This suggests that cell proliferation had not yet been fully initiated or that the material surfaces were still insufficiently favorable to support sustained cell attachment and growth at this stage.

Peak cell numbers on day 14 were recorded for the PLA/HA_10 and PLA/HA_20 composites (Figure 8b). These results indicate that cells in these groups successfully adhered to the material surface and progressed into the proliferative phase.

By day 21, the PLA/HA_20 group exhibited the highest cell count, while the PLA/HA_10 group maintained a considerable number of viable cells (Figure 8b), further corroborating effective cell proliferation on these surfaces. In contrast, the PLA/HA_30 and PLA/HA_40 samples exhibited reduced cell numbers at both day 14 and day 21. Notably, the PLA/HA_40 group showed a decline from an initial peak on day 1 to subsequent time points (i.e., days 14 and 21, Figure 8b). These results suggest that, although higher HA content may initially enhance cell adhesion, it appears to hinder long-term cell proliferation, potentially due to unfavorable surface properties or excessive ionic release.

Overall Assessment of Biological Performance:

Overall, the observed cell viability values were within an acceptable range for all tested PLA/HA composites. However, the PLA/HA_10 and PLA/HA_20 samples exhibited superior cytocompatibility. At these concentrations, both cell viability (as indicated by absorbance values) and cell proliferation (as reflected by live cell counts) were consistently enhanced. Among all formulations, the PLA/HA_20 samples demonstrated the most favorable biological response on day 21 (Figure 8a,b). In contrast, increasing the HA content to 30% or higher led to diminished biological performance. This decline may be attributed to factors such as calcium ion imbalance, excessive surface stiffness, or local pH alterations induced by the high HA concentration, all of which can adversely affect cellular adhesion and proliferation.

4. Conclusions

This study investigated the mechanical, structural, and cytocompatibility properties of polylactic acid (PLA) filaments containing different ratios of hydroxyapatite (HA) (i.e., 10, 20, 30, and 40 wt.%) to assess their suitability for artificial bone tissue applications. The findings demonstrate that HA content plays a decise role in determining the overall performance of PLA/HA filaments, influencing not only their mechanical and structural characteristics but also their biological response over time. In terms of both strength and flexibility, the PLA/HA_10 filaments exhibited mechanical properties most comparable to those of natural bone tissue. The PLA/HA_20 filaments also demonstrated relatively high elasticity while maintaining acceptable strength. In contrast, the PLA/HA_30 and PLA/HA_40 filaments displayed moderate to low stiffness and strength, accompanied by a pronounced increase in brittleness. These results suggest that higher HA contents compromise the ductility of the material, a property that is critical for applications requiring an optimal balance between strength and toughness. Examination of the surface properties revealed that the PLA/HA_10 and PLA/HA_20 filaments exhibited the most favorable mechanical performance and biological responses, including osteoblast adhesion and proliferation. Deviations from these optimal HA ratios were shown to compromise both the mechanical strength and the cytocompatibility of the composites. Notably, in both cases, cytocompatibility was further enhanced after 14 and 21 days of in vitro culture, confirming the potential suitability of these filaments for applications in artificial bone tissue engineering. Future research should focus on further improving these outcomes by optimizing filament fabrication parameters and incorporating additional functional additives. This study demonstrates that HA-doped PLA filaments consitute a promising strategy for the development of scaffolds for artificial bone tissue engineering. Notably, incorporation of 10–20 wt.% HA into the PLA matrix provides an optimal balance between mechanical strength and biological performance, rendering these composites as suitable candidates for mimicking the properties of native bone tissues.

10.57647/pibm.2025.17542

Statements & Declarations

Funding
No funding was received to assist with the preparation of this manuscript.

Ethics approval
This article does not contain any studies with human participants or animals performed by any of the authors.

Acknowledgments
L.D. acknowledges with thanks the support of this work by the Romanian Ministry of Education and Research, under Romanian National Nucleu Program LAPLAS VII Contract No. 30N/2023.

Authors Contribution

Conceptualization: Bilal Cinici, Oguzhan Gunduz; Methodology: Sule Gozonunde, Mustafa Kurt; Formal analysis and investigation: Bilal Cinici, Sule Gozonunde, Mustafa Kurt, Liviu Duta, Oguzhan Gunduz; Writing - original draft preparation: Bilal Cinici, Liviu Duta, Oguzhan Gunduz; Writing - review and editing: Bilal Cinici, Sule Gozonunde, Mustafa Kurt, Liviu Duta, Oguzhan Gunduz; Funding acquisition: Liviu Duta; Resources: Liviu Duta, Oguzhan Gunduz; Supervision: Liviu Duta, Oguzhan Gunduz. All authors have read and approved the final version of the manuscript.

Availability of data and materials

The datasets generated during and/or analysed during the current study are available from the corresponding authors on reasonable request.

Conflict of interests

The authors have no relevant financial or non-financial interests to disclose.

References

[1] Francis A. Biological evaluation of preceramic organosilicon polymers for various healthcare and biomedical engineering applications: a review. J Biomed Mater Res B Appl Biomater. 2021;109(5):744-764. doi:10.1002/jbm.b.34740

[2] Beheshtizadeh N, Azami M, Abbasi H, Farzin A. Applying extrusion-based 3D printing technique accelerates fabricating complex biphasic calcium phosphate-based scaffolds for bone tissue regeneration. J Adv Res. 2022;40:69-94. doi:10.1016/j.jare.2021.12.012

[3] Alonzo M, Primo FA, Kumar SA, Mudloff JA, Dominguez E, Fregoso G, Ortiz N, Weiss WM, Joddar B. Bone tissue engineering techniques, advances, and scaffolds for treatment of bone defects. Curr Opin Biomed Eng. 2021;17:100248. doi:10.1016/j.cobme.2020.100248

[4] Zhang L, Yang G, Johnson BN, Jia X. Three-dimensional (3D) printed scaffold and material selection for bone repair. Acta Biomater. 2019;84:16-33. doi:10.1016/j.actbio.2018.11.039

[5] Ilyas RA, Zuhri MYM, Aisyah HA, et al. Natural fiber-reinforced polylactic acid, polylactic acid blends and their composites for advanced applications. Polymers. 2022;14(1):202. doi:10.3390/polym14010202

[6] Chen H, Han Q, Wang C, Liu Y, Chen B, Wang J. Porous scaffold design for additive manufacturing in orthopedics: a review. Front Bioeng Biotechnol. 2020;8:609. doi:10.3389/fbioe.2020.00609

[7] Roohani-Esfahani SI, Newman P, Zreiqat H. Design and fabrication of 3D printed scaffolds with a mechanical strength comparable to cortical bone to repair large bone defects. Sci Rep. 2016;6:19468. doi:10.1038/srep19468

[8] Wu D, Spanou A, Diez-Escudero A, Persson C. 3D-printed PLA/HA composite structures as synthetic trabecular bone: a feasibility study using fused deposition modeling. J Mech Behav Biomed Mater. 2020;103:103608. doi:10.1016/j.jmbbm.2019.103608

[9] Wang W, Zhang B, Zhao L, et al. Fabrication and properties of PLA/nano-HA composite scaffolds with balanced mechanical properties and biological functions for bone tissue engineering application. Nanotechnol Rev. 2021;10(1):1359-1373. doi:10.1515/ntrev-2021-0083

[10] Åkerlund E, Diez-Escudero A, Grzeszczak A, Persson C. The effect of PCL addition on 3D-printable PLA/HA composite filaments for the treatment of bone defects. Polymers. 2022;14(16):3305. doi:10.3390/polym14163305

[11] Orozco-Díaz CA, Moorehead R, Reilly GC, Gilchrist F, Miller C. Characterization of a composite polylactic acid-hydroxyapatite 3D-printing filament for bone-regeneration. Biomed Phys Eng Express. 2020;6(2):025007. doi:10.1088/2057-1976/ab73f8

[12] O'Brien FJ. Biomaterials & scaffolds for tissue engineering. Mater Today. 2011;14(3):88-95. doi:10.1016/S1369-7021(11)70058-X

[13] Kumar A, Nune KC, Murr LE, Misra RDK. Biocompatibility and mechanical behaviour of three-

dimensional scaffolds for biomedical devices: process–structure–property paradigm. Int Mater Rev. 2016;61(1):20-45. doi:10.1080/09506608.2015.1128310

[14] Ghilan A, Chiriac AP, Nita LE, et al. Trends in 3D printing processes for biomedical field: opportunities and challenges. J Polym Environ. 2020;28:1345-1367. doi:10.1007/s10924-020-01722-x

[15] Elsen SR, Mahendran T, Atkare PP, Bhosale AA. Fabrication of bio-scaffold by additive manufacturing technique for bone synthesis using generative design. IOP Conf Ser Mater Sci Eng. 2021;1123(1):012068. doi:10.1088/1757-899X/1123/1/012068

[16] Wu J, Qian X, Wang MY. Advances in generative design. Comput Aided Des. 2019;116:102733. doi:10.1016/j.cad.2019.102733

[17] Kanwar S, Vijayavenkataraman S. Design of 3D printed scaffolds for bone tissue engineering: a review. Bioprinting. 2021;24:e00167. doi:10.1016/j.bprint.2021.e00167

[18] Chocholata P, Kulda V, Babuska V. Fabrication of scaffolds for bone-tissue regeneration. Materials. 2019;12(4):568. doi:10.3390/ma12040568

[19] Foroughi AH, Valeri C, Razavi MJ. A review of computational optimization of bone scaffold architecture: methods, challenges, and perspectives. Prog Biom Eng. 2024;7:012003. doi:10.1088/2516-1091/ad879a

[20] Gao W, Zhang Y, Ramanujan D, et al. The status, challenges, and future of additive manufacturing in engineering. Comput Aided Des. 2015;69:65-89. doi:10.1016/j.cad.2015.04.001

[21] Taib NAAB, Rahman MR, Huda D, et al. A review on poly lactic acid (PLA) as a biodegradable polymer. Polym Bull. 2023;80(2):1179-1213. doi:10.1007/s00289-022-04160-y

[22] Ebrahimi F, Ramezani Dana H. Polylactic acid (PLA) polymers: from properties to biomedical applications. Int J Polym Mater Polym Biomater. 2022;71(15):1117-1130. doi:10.1080/00914037.2021.1944140

[23] Unal S, Oktar FN, Mahirogullari M, Gunduz O. Bone structure and formation: a new perspective. In: Bioceramics. Elsevier; 2021:175-193. doi:10.1016/B978-0-08-102999-2.00009-0

[24] Collins MN, Ren G, Young K, Pina S, Reis RL, Oliveira JM. Scaffold fabrication technologies and structure/function properties in bone tissue engineering. Adv Funct Mater. 2021;31(21):2010609. doi:10.1002/adfm.202010609

[25] Cinici B, Yaba S, Kurt M, Yalcin HC, Duta L, Gunduz O. Fabrication strategies for bioceramic scaffolds in bone tissue engineering with generative design applications. Biomimetics. 2024;9:409. doi:10.3390/biomimetics9070409

[26] Wijerathne HS, Yan D, Zeng B, et al. Effect of nano-hydroxyapatite on protein adsorption and cell adhesion of poly(lactic acid)/nano-hydroxyapatite composite microspheres. SN Appl Sci. 2020;2:1-8. doi:10.1007/s42452-020-2531-8

[27] Rao SH, Harini B, Shadamarshan RPK, Balagangadharan K, Selvamurugan N. Natural and synthetic polymers/bioceramics/bioactive compounds-mediated cell signalling in bone tissue engineering. Int J Biol Macromol. 2018;110:88-96. doi:10.1016/j.ijbiomac.2017.09.029

[28] Martinez-Marquez D, Mirnajafizadeh A, Carty CP, Stewart RA. Application of quality by design for 3D printed bone prostheses and scaffolds. PLoS One. 2018;13(4):e0195291. doi:10.1371/journal.pone.0195291

[29] Zhang B, Wang L, Song P, et al. 3D printed bone tissue regenerative PLA/HA scaffolds with comprehensive performance optimizations. Mater Des. 2021;201:109490. doi:10.1016/j.matdes.2021.109490

[30] Hasanzadeh R, Mihankhah P, Azdast T, Rasouli A, Shamkhali M, Park CB. Biocompatible tissue-engineered scaffold polymers for 3D printing and its application for 4D printing. Chem Eng J. 2023;476:146616. doi:10.1016/j.cej.2023.146616

[31] Hasanzadeh R, Azdast T, Mojaver M, Darvishi MM, Park CB. Cost-effective and reproducible technologies for fabrication of tissue engineered scaffolds: the state-of-the-art and future perspectives. Polymer. 2022;244:124681. doi:10.1016/j.polymer.2022.124681

[32] Custodio CL, Broñola PJM, Cayabyab SR, Lagura VU, Celorico JR, Basilia BA. Powder loading effects on the physicochemical and mechanical properties of 3D printed poly lactic acid/hydroxyapatite biocomposites. Int J Bioprint. 2021;7(1):326. doi:10.18063/ijb.v7i1.326

[33] Bernardo MP, da Silva BCR, Hamouda AEI, et al. PLA/hydroxyapatite scaffolds exhibit in vitro immunological inertness and promote robust osteogenic

differentiation of human mesenchymal stem cells without osteogenic stimuli. Sci Rep. 2022;12:2333. doi:10.1038/s41598-022-05207-w

[34] Kaczmarek H, Nowick M, Vuković-Kwiatkowska I, Nowakowska S. Crosslinked blends of poly(lactic acid) and polyacrylates: AFM, DSC and XRD studies. J Polym Res. 2013;20:1-12. doi:10.1007/s10965-013-0091-y

[35] Mathieu LM, Mueller TL, Bourban PE, Pioletti DP, Müller R, Månson JAE. Architecture and properties of anisotropic polymer composite scaffolds for bone tissue engineering. Biomaterials. 2006;27(6):905-916. doi:10.1016/j.biomaterials.2005.07.015

[36] Murariu M, Galluzzi A, Paint Y, et al. Pathways to green perspectives: production and characterization of polylactide (PLA) nanocomposites filled with superparamagnetic magnetite nanoparticles. Materials. 2021;14:5154. doi:10.3390/ma14185154

[37] Bernardes GP, Andrade MP, Poletto M, Luiz NR, Santana RMC, Forte MMdC. Evaluation of thermal decomposition kinetics of poly(lactic acid)/ethylene elastomer blends. Polymers. 2023;15:4324. doi:10.3390/polym15214324

[38] Pandele AM, Comanici FE, Carp CA, et al. Thermal and mechanical behavior of cellulose acetate–hydroxyapatite micro- and nano-composites obtained by an eco-friendly approach. Materials. 2020;13(2):274. doi:10.3390/ma13020274

[39] Lyu S, Huang C, Zhang X, Li H. Effect of thermal processing on the crystallization behavior of PLA/HA composites. J Appl Polym Sci. 2019;136(18):47452. doi:10.1002/app.47452

[40] Dal Poggetto G, D'Amora U, Ronca A, Raucci MG, Soriente A, d'Ayala GG, Laurienzo P. Chemical modification of PLA for the design of 3D printed nanocomposite scaffolds with enhanced degradability for bone tissue engineering. Polym Composite. 2025;46(9):7964-7980. doi:10.1002/pc.29470

[41] Bose S, Roy M, Bandyopadhyay A. Recent advances in bone tissue engineering scaffolds. Trends Biotechnol. 2012;30(10):546-554. doi:10.1016/j.tibtech.2012.07.005

[42] Azdast T, Hasanzadeh R. Polylactide scaffold fabrication using a novel combination technique of fused deposition modeling and batch foaming: dimensional accuracy and structural properties. Int J Adv Manuf Technol. 2021;114:1309-1321. doi:10.1007/s00170-021-06915-9

[43] Aghaiee S, Azdast T, Hasanzadeh R, Farhangpazhouh F. Fabrication of bone tissue engineering scaffolds with a hierarchical structure using combination of 3D printing/gas foaming techniques. J Appl Polym Sci. 2024;141(16):e55238. doi:10.1002/app.55238

[44] Rasouli A, Azdast T, Mohammadzadeh H, et al. Morphological properties and mechanical performance of polylactic acid scaffolds fabricated by a novel fused filament fabrication/gas foaming coupled method. Int J Adv Manuf Technol. 2022;119:7463-7474. doi:10.1007/s00170-022-08743-x